

A New Method for Estimating the Absolute Magnitude Frequency Distribution of Near Earth Asteroids (NEAs)

F. Valdes^a

^a*National Optical Astronomy Observatory, P.O. Box 26732, Tucson, AZ 85732*

Abstract

The distribution of solar system absolute magnitudes (H) for the near-Earth asteroids (NEAs) observable near opposition – i.e. Amors, Apollos, and Atens (A^3) – is derived from the set of **ALL** currently known NEAs. The result is based only on common sense assumptions of uniformly random distributions and that the orbital phase space and H -magnitude distribution of known NEAs is representative of the total population. There is no population or other modeling and no assumption on albedo except in interpreting the result as a size-frequency distribution (SFD). The analysis is based on the 18355 A^3 NEAs cataloged by the MPC as of June 2018. The observations from 9 of the top programs (in terms of number of distinct NEAs observed) and the smaller but deeper DECam NEO Survey are used, comprising 74696 measurements of 13466 NEAs observed within 30 deg of opposition. The only parameter in the analysis is an estimate of the detection magnitude limits for each program.

A single power-law slope for the cumulative distribution, $\log(N < H) = 0.50 \pm 0.03H$, for $H < 27$ is found with no evidence for additional structure. A turn-over fainter than 27th magnitude may occur, but the population of known NEAs is dropping off rapidly because they are difficult to detect and so possibly is a completeness effect. Connecting to the nearly complete census of the brightest/biggest NEAs (diameter $> \sim 2\text{Km}$) provides a normalization that estimates $\sim 10^8 A^3$ NEAs with $H < \sim 27$ corresponding to NEAs greater than $\sim 10\text{m}$ in diameter for reasonable typical albedos.

Restricting the analysis to Earth crossing asteroids (10839 known, 7336 selected, 36541 observed) produces the same power-law slope.

Keywords: Asteroids, NEO, NEA, HFD, SFD

1. Introduction

The most basic question in the study of near-Earth objects (NEOs) is the size of the population and how it is distributed by mass. Answering this question has important relevance to solar system science. It also has ramifications beyond this

Email address: fvaldes@noao.edu (F. Valdes)

science domain because of the potential consequences of impacts with the Earth causing damage, and worse, to the inhabitants of our planet. This has led to a focus on this basic question by governments, such as in the U.S. congressional mandate (in the NASA Authorization Act of 2005 and the detailed study of Stokes et al. [10]) to measure the number of NEOs in the hazardous, if not catastrophic, range – defined as diameters greater than 140 meters.

The observational version of this question is not the mass or size distribution but the absolute solar system magnitude, or H -magnitude, frequency distribution (HFD). Size or mass distributions are derived from this with considerably more assumptions and interpretation. This paper estimates the near-Earth asteroid (NEA) HFD with Amor, Apollo, and Aten (A^3) orbits using a new method based solely on observations that avoids population models and simulations.

As for all studies, the starting point is the catalog of known near-Earth asteroids (NEAs). The catalog used here is that tabulated by the Minor Planet Center [8] as of June 2018. In order to be in this catalog an object must have met the MPC criteria needed to determine an orbit and absolute solar system magnitude as well as the adopted definitions for the NEA classes. In addition to orbital parameters, this catalog includes the individual measurements and attributions to the programs reporting them.

The notable results reported in this paper are 1) an HFD that is a simple power law and 2) the difference in estimated number of NEAs, in the range of interest for planetary defense, between this purely observational method and the studies of Harris and D’Abramo [6], Schunová-Lilly et al. [9], Granvik et al. [4], and Tricarico [11] (henceforth HSGT) using various other methods. In particular, the HSGT studies predict a factor of approximately seven fewer NEAs with diameters larger than the congressional objective than found in this study. Clearly this is significant for understanding the feasibility of mapping these NEAs.

In this paper we describe the method in §2 and its application to the catalog of known NEAs in §3. Section 4 discusses the results in light of the other estimates of the HFD and the implication for satisfying the planetary defense mandate for 140m and larger NEAs.

2. The Method

The method presented in this paper considers the problem of estimating the absolute solar system magnitude frequency distribution of near-Earth asteroids from a purely observational perspective. The dominant factor in this problem is the volume correction factor; that is, given an observed sample of NEAs what fraction of the true population was in the observable volume vs the volume that was unobservable? In observational methodology this is known as the Malmquist bias [7].

Why is this the dominant factor and not things like detection efficiencies? Because the concept of near-Earth asteroids, and how they are defined as a class, focuses on “near by” and the perihelia boundary at 1.3 AU and it is

easy to forget that these asteroids typically have aphelia that put them far from the Earth during most of their orbit. This puts them beyond the current observational limits of the telescopes for considerable periods of time.

Fortunately, the unobservable population of NEAs can be accounted for without population modeling and significant assumptions. This is because orbital mechanics tells us the probabilities of where NEAs can be provided we have the orbital parameters. By definition NEAs have those parameters in order to be classified as such. This is the basis of the methodology presented in this paper.

Figures 1 and 2 illustrate this point. These show the distribution of orbital and H -magnitude parameters for the known NEAs. In figure 1 the aphelia distances for the known NEAs are shown as a function of perihelion distance and in figure 2 as a function of absolute magnitude. What can be seen in these scatter plots is that aphelion distances extend to 5 AU and beyond. In figure 2 the solid line is particularly telling in showing the boundary of distances at which NEAs are observed (in this case by Pan-STARRS). This illustrates that NEAs are only observable for a small part of their orbit.

2.1. Assumptions

Since what is being done is estimating what is not observed from what is known some assumptions must be made. The believability of the result depends on the reasonableness and number of assumptions. The method presented here is based on a very small set of assumptions that are hard to dispute and are almost axiomatic.

The most important assumption is that *the population of known NEAs is representative of the true population* that we are trying to estimate. This includes the range and relative frequency of orbital and H -magnitude parameters in the distribution of known NEAs. It seems almost axiomatic since how are we to estimate something that is completely unknown?

The second assumption is that *the orbital phase of the NEAs in the true population is uniformly distributed*; in orbital parlance, the mean anomalies are uniformly random. In plain words, a NEA is equally likely to be found anywhere along its orbit independent of any other NEA or time of observation.

The final assumption, that is also almost axiomatic, is that *using the largest set of observations possible averages out a variety of sins*. In particular, the variability of magnitudes, due both to physical rotation and measurement errors, is averaged out. In the data used in this study NEAs typically have multiple observations by the same program and by multiple programs and at a variety of epochs.

A key factor in this study is that it is specifically about the shape of the distribution and whether a power law is sufficient to describe the shape. The absolute numbers are set by a normalization to the biggest NEAs that are considered to be 95%, or some similar number, complete. The importance of this is that most of the concerns about differences in programs are subsumed by the normalization.

2.2. *Input Quantities and Method Parameters*

For all (ground-based) NEA programs the primary observational constraint on the volume searched is their apparent magnitude limit. This is almost the *only* parameter in the method presented in this paper.

The basic input to the method are the measured quantities of magnitude and time of an observation. In principle, any observation of a NEA can be used provided there is an estimate of the magnitude limit for the observation.

The remaining input parameters are the orbital parameters which provide a distance for the observation and the absolute magnitude H for the NEA. Note that these are also observational quantities in that they are derived directly from reported observations and the axiomatic laws of orbital mechanics.

The magnitude limit of a particular observation is a fuzzy quantity and is variable due to weather conditions. However, the principle that over a large body of observations there is a typical limit to which the statistics converge applies. The effect of uncertainties in this magnitude limit can and is explored by applying the the analysis with a range of values.

There is also the question about detection probability for a particular NEA. It will be shown that this is a small effect.

In this version of the method, observations are limited to be near opposition. This is in order to apply a simple inverse-square scaling for magnitudes. In principle the method can be extended to all observations with the application of a geometric correction for illumination phase. However, it is conceptually and analytically simpler to make this restriction. It also the case that most NEO detection and recovery programs primarily observe near opposition for the obvious reasons of maximum brightness and use of the full night.

2.3. *Method in Words*

Each NEA observation is considered a sample from the class of all NEAs with nearly identical orbital and absolute magnitude properties. In this class all positions along the orbit are assumed to be occupied with a uniform probability distribution in time. We also assume that there is no preferred orientation of the orbit (i.e. the longitude of the ascending node and the argument of periapsis). The inclinations are not uniform but what is required is that the observed NEAs sample the inclinations in the same way as the full population would be sampled in the absence of magnitude limits.

The assumption that there is no preferred orientation is important. This means we can conceptually orient each point along an orbit so that it is within the same observation window as the specific representative NEA. In other words, each potential NEA distance from the full population is from a different orientation of the same elliptical orbit and this is equivalent to sampling each point in the orbit at different times. This is a stationary stochastic approach where orientation is traded with time. This concept allows evaluating the probability of NEAs with similar orbits to be observed at different distances and, therefore, different magnitudes, rate of apparent motion, and time spent within and outside the window of observability.

Each NEA is generally observed multiple times and usually by multiple programs. Given the time of observation and the orbital parameters a geocentric distance is computed. Given the apparent and limiting magnitude of the observation, the maximum observable geocentric distance is computed. This is purely an inverse square law scaling calculation and the albedo does not enter. If the analysis is limited to observations near opposition, which we do in this paper, any phase effect can be ignored. This is a key point that NEA size or albedo don't need to be known and everything related to apparent magnitudes simply scale geometrically.

As long as the sample also includes all the absolute magnitudes with their representative orbits, there is also no inherent dependence on H in the method. This is key to the primary goal of determining the shape of the HDF. All the other factors which are not magnitude dependent end up in the normalization set by asymptoting to the nearly complete bright and large NEAs.

2.4. Method in Figures

Figure 3 illustrates the key concepts. The ensemble of similar orbits (a) shows that when we describe a NEA as being found anywhere in its orbit and observed at opposition it is not the exact same orbit but one whose orientation (i, Ω, ω) is such as to be in the opposition cone. The observable and unobservable volumes and the opposition cone are shown by the broken lines. In the cartoon one NEA is shown in the observable volume and three outside but bounded by the aphelion of the orbit.

The second diagram (b) shows the distribution of heliocentric distances for the orbit when NEAs are equally likely to be anywhere in their orbit. As just mentioned, no single NEA traces a radial distribution of distances observed at opposition but it is the ensemble of like NEAs that would have this distribution. The limitation to near opposition allows interpretation of the heliocentric distances as geocentric distances with magnitudes (for an identical NEA) scaling by the inverse square law without worrying about the illumination phase. The dashed lines correspond to the Earth's orbit and the maximum observable distance, for a given observed magnitude, set by the magnitude limit of the observation.

As in the figure, the time weighted 1D distance ratio is determined by computing a list of geocentric distances sampled uniformly in time. Adding up the number of points between the Earth and the distances defined by the aphelion and limiting magnitude and taking the ratio gives the time weighted radial factor. In the example the percentages shown are the fraction of the time, equivalent to the fraction of NEAs in the ensemble, which are within the regions. The ratio of the percentage outside the Earth to what is observable in this example, 71%/26%, is the 1D volume factor. One can think of this as a stretched ratio of the distance in the opposition cone. As a purely geometric behavior, the cube of this 1D ratio gives the desired volume ratio. Note that geometrically it doesn't really matter if the observing program is truly a cone.

2.5. Method in Equations

For each observation i of NEA j by subsample k of program p near opposition, the distance from the Earth, d_{ijk} , at which it was observed is computed from the time of observation and its derived orbital parameters. The concept of subsamples is used to evaluate the uncertainties by considering the scatter in the results across the subsamples in a program and across all programs.

In this derivation d denotes the distance from the Earth and r is the heliocentric distance. By restricting the observations to near opposition we use the approximation $d = r - 1$ where we consistently use AU as the distance unit. Note that a *program* is defined to be with a single filter and consistent observational protocol.

The inverse square law and the observed apparent magnitude m_{ijk} for the opposition observation allows computing $d(m)$ and $m(d)$ for all NEAs having a similar orbit and absolute magnitude and observed within the same opposition window.

$$d(m) = d_{ijk} 10^{0.2*(m-m_{ijk})}, m(d) = m_{ijk} + 5 \log(d/d_{ijk}) \quad (1)$$

Note that this purely geometric relationship is not dependent on any assumptions about albedo or the filter. Of special significance is $d(\tilde{m}_{ijk})$ which is the distance to which a similar NEA could be observed with the limiting magnitude \tilde{m}_{ijk} for the observation. In the application of the method we make the simplification that all observations of all NEAs by a particular program are the same and so the limiting magnitude is \tilde{m}_k .

Another magnitude dependent factor is the detection probability distribution, $P_k(d(m)) = P_k(m(d), v(d))$ where $v(d)$ is the apparent rate of motion which is a property of the orbit largely governed by the distance. As with the limiting magnitude this is simplified by assuming P is the same for all observations and NEAs of the same program. In the absence of information about the detection probability distribution we use $P_k \equiv 1$. The consequence of this is discussed in §3.2.

To estimate the number of NEAs with these orbital parameters consider the family of orbits where such a NEA is uniformly distributed along the orbit and, at each point, the orbit is oriented such that the NEA would appear near opposition. This is described by the function $t(d(M))$ where $d(M)$ is the geocentric distance of a NEA as a function of the mean anomaly M , and $t(d)$ is the time spent at that distance. The importance of this is that uniformly distributed in mean anomaly is equivalent to uniform in time around the orbit but the time spent at a particular heliocentric distance is not uniform; asteroids spend more time near aphelion than perihelion. As noted previously, near opposition heliocentric and geocentric distances are simply related. Figure 3b provides a particular example of $t(d(M))$ by considering the density of points in distance where the points are uniformly spaced in mean anomaly.

For this uniform distribution in mean anomaly, arranged such that $d = r - 1$, the integral of the time spent at each distance over the observable part of the orbit relative to the whole orbit contributes to the volume correction factor.

$$z_j = \int_{d_{min}}^{Q-1} t(d_j(M))dM / \int_{d_{min}}^{d_{max}(\tilde{m})} P(d_j(M))t(d_j(M))dM \quad (2)$$

where d_{min} is the minimum distance for observing the NEA, $Q - 1$ is the maximum distance for the orbit ($Q =$ aphelion distance), and $d_{max}(\tilde{m}) (= \min[d(\tilde{m}), Q - 1])$ is the maximum distance a program could detect a NEA. While d_{min} is ideally zero it is a parameter because detections very near the Earth are highly uncertain in magnitude and extrapolation to the entire orbit is problematic.

Equation 2 is expressed in this somewhat indirect way to motivate the way it is calculated numerically in application. A table of discrete distances in uniform steps of M is computed from Kepler's formulas. This is conceptually like a large sample of NEAs placed along the orbit in uniform steps of mean anomaly. The integrals are then sums of this population over the distance limits and the ratio is the number potentially observable verse the number tabulated. Again, fig. 3b illustrates this.

A way to think of z is that it is a non-linear stretch of the volume that accounts for the variation of the time a NEA spends within the visible and invisible portion of its orbit rather than simply using the geometric distance ratio $z_{geo} = (Q - 1 - d_{min}) / (d(\tilde{m}) - d_{min})$. Equation 2 reduces to this geometric factor if t and P are constant. Another way to think of it is as the fraction of time a NEA is observable with a magnitude limit \tilde{m} relative to an infinitely deep magnitude limit with a perfect detection probability ($P = 1$).

Taken as a stretch in the distance of the observation cone the volume factor for an instance of a NEA is then $V_{ijk} = (z_{ijk})^3$.

There is one final factor to consider. The fraction, f_j , of known NEAs observed by a program for each asteroid type in the population. For example, if a program sample included 100% of the known $H = 17.3$ (~ 1 km) asteroids but only 10% of the $H = 22$ (~ 100 m) ones then $f = 1$ and $f = 0.1$ respectively. This factor allows each program subsample to estimate the result for the same complete known NEA catalog. Note this factor is different than P , the probability of detecting an asteroid at different distances given an observation.

Another way to understand f is that if a program had the sensitivity to reach the entire orbital volume of every NEA that it observed, where all V_{ijk} would be one, then the computed distribution would converge to the known NEA population.

The estimate of the cumulative absolute magnitude distribution, C , for a program subsample is given by

$$C_k(H) = \left\{ \sum_j^{H_j < H} \left(\frac{\sum_i V_{ijk}}{N_{jk}} \right) / f_k(H_j) \right\} / A_k = \left\{ \sum_j^{H_j < H} \overline{V}_{jk} / f_k(H_j) \right\} / A_k. \quad (3)$$

The inner sum is the average of the estimates for a particular NEA from multiple observations and recoveries of the NEA in a program subsample; which we

denote as $\overline{V_{jk}}$. The observations themselves may already be an average for each night. The outer sum is the cumulative value over the absolute magnitudes where each NEA j has an assigned H_j as part of their catalog parameters.

A_k is a normalization characteristic of the program related to the effective volume (in space, time, effective depth, etc.) as well as the detection probability normalization. It is determined by reproducing the known distribution of bright/large NEAs in the program where the incompleteness approaches zero. The fact that there is this arbitrary normalization is why the principle, observationally derived, quantity in this study is the shape of the absolute magnitude distribution. However, a well constrained shape tied to the known distribution does provide a well constrained absolute distribution and most studies of the NEA population ultimately have some similar normalization to the known bright NEAs.

There are various ways equation 3 could be applied. In this study we will compute $C_k(H_m)$ where H_m are in discrete bins. As will be shown, over the biggest programs the $C_k(H_m)$ are very similar. While one could, in principle, use all the $\overline{V_{jk}}$ in a sum across programs in eq. 3, in this study a final absolute magnitude distribution is derived by averaging $C_k(H_m)$ ($= \overline{C}(H_m)$) across a program or over all programs at each bin m and using the standard deviation to evaluate the uncertainties.

3. Application

The method for estimating the absolute magnitude frequency distribution described in the preceding section is applied to the catalog of known NEAs available from the Minor Planet Center in June 2018. In §3.1 the statistics of the available data and the selection of programs and subsamples is presented. In §3.2 details of how the method was applied and the results are described.

The believability of this study is gauged by considering the robustness and uncertainties of the result along with Occam’s razor. The discussion notes variations that were tried; all leading to the same answer. Also §3.3 considers a simple experiment demonstrating the result obtained is not preordained by the method regardless of the input information.

The analysis was all done in SQL (structured query language) with a database constructed from all the observations and parameters of the known NEAs. This allows many tests to be done and repeating the analysis when the catalog of known NEAs expands over time.

3.1. Data Selection

The catalog obtained from the MPC in June 2018 contains 18,355 NEAs observed by 1,670 distinct combinations of MPC program identifiers and filter, which we call a program ID or simply a program. As described previously, the analysis is simpler if we consider only NEAs observed near opposition, chosen as within 30 degrees in ecliptic longitude, which gives 16,313 NEAs. The analysis was also done with a 20 degree opposition limit with identical results though,

of course, with a smaller sample. Hence, the result is not sensitive to the exact value of the opposition window.

We further select a limited number of programs for this initial analysis. There are two reasons for this. First, a small number of well known programs account for the majority of NEA discovery/recovery observations. Second, while in principle any observation can be used in the analysis, the requirement that each observation have an associated magnitude limit leads to programs with a large number of observations allowing solid estimates of magnitude limits as demonstrated later by figure 4.

The programs were chosen by sorting the number of distinct NEAs observed by each program in the catalog and selecting 9 of the top 13 programs. In addition, the DECam NEO Survey of Allen et al. [1] was included because of its greater depth and the availability of detection efficiency curves to check if these are important to the result. The sorted list is shown in table 1. This also shows the number of nights with observations N_{night} . There are normally 3 or more measurements of a NEA over a short time span in a night and in this analysis those measurements are averaged to define a single "observation-night". The consideration is that the observed distance and magnitude, the primary inputs to the method, do not change significantly in these reports and so give a better estimate for a particular epoch of observation.

Table 1 also shows the 10 programs are divided into two sets where set 1 is the top 5 programs plus the DECam NEO Survey and set 2 is the remaining selected programs.

The net result of these selections is that 13,466 NEAs from 10 programs with 74,696 observation nights are included in this study. This achieves a key goal of this study to use a substantial subset of all known NEAs and NEA observations.

A subset of this dataset restricted to Earth crossing asteroids (ECAs) was also analyzed with identical results, though we don't present specific figures. This subset of Apollo and Aten asteroids consisted of 7,334 (out of 10,839) with 36,541 observation-nights.

The distribution of the selected NEAs in (q, Q) space, perihelion and aphelion distance, is shown in figure 1 for those selected and those not selected. These figures speak to several points made in this paper: 1) a large fraction of the known NEAs are used and 2) there is no qualitative difference between the NEAs used and not used. The second point relates to the key assumption that the NEAs in the analysis form an unbiased sample of the known and full population of NEA orbits.

The key, and almost sole, parameter in the analysis is a magnitude limit, \tilde{m}_k , for each observation. The advantage of programs with large numbers of consistent observations is that a magnitude limit can be estimated by looking at the distribution of observed apparent magnitudes reported. Figure 4 shows the observed and H -magnitudes for each program. The key features of these plots are that all programs, regardless of telescope aperture, sample the range of H -magnitudes and that the upper limit of apparent magnitudes has a reasonably clear boundary. This boundary defines a magnitude limit with little dependence on NEA absolute magnitude. In this figure, and all other figures showing scatter

plots of the observations as a function of absolute magnitude, note the lack of obvious differences in the range $H=[20:26]$ where the HSGT studies find a different character from other parts of the range.

The figure shows lines for two magnitude limits used in the analysis. Table 1 provides the adopted fainter limit (the upper line). The second magnitude limit is simply 0.5 magnitude brighter. Two limits are used to investigate the robustness of the results with the choice of magnitude limit and as a way to bound the unknown detection probabilities (discussed later and illustrated by figure 5).

Program H21V appears unusual in the figure because two telescopes of different apertures are used to make observations depending on the expected apparent magnitude. We set a magnitude limit, as with the other programs, and then checked if the analysis showed any peculiarities with respect to the other programs. The results for just this program were found not to be significantly different than the other programs. One could argue that this is expected to be the case since this is a recovery program rather than a discovery program.

In order to gauge the uncertainties and robustness of the result the scatter in many programs and subsamples from the programs are used in the analysis. In other words, any subsample of the known set of NEAs, providing that each samples the range of properties (H -magnitudes and orbits), should give the same HFD apart from uncertainties in the measurements and program techniques. The scatter in the resultant HFDs provides a measure of the uncertainties and variations in the data which is a stand-in for the largely unknowable uncertainties in all aspects of NEA discovery and recovery programs.

We've already identified two types of subsamples – by program and by applying different magnitude limits. In the results of the following section we take 20 subsamples of the NEAs observed by a program where each subsample contains a random selection of half of the NEAs. Ten of these subsamples were analyzed with the magnitude limit given in table 1 and the other ten with a limit that is a half magnitude brighter.

We note that an exploratory analysis was done with just a single sample of all NEAs observed by each program and with a single magnitude limit. The results reported here with the subsamples are effectively the same but with a clearer picture of the uncertainties.

What does varying the magnitude limit represent? As seen in the detailed derivation of the method there should be a factor for the detection probability of a NEA at various points along its orbit. In terms of the observational factors that govern the probabilities (beyond those imposed by the atmosphere which are stochastic) these are primarily the apparent magnitude and rate of motion which directly relate.

Detection probabilities generally have a shape that goes from high probability to zero as the apparent magnitude approaches the magnitude limit. Figure 5 illustrates the idea with a cartoon representation of a detection probability curve in apparent magnitude. Since we lack detailed knowledge of the detection probabilities for all but the DECam NEO Survey we are effectively representing the probabilities as a step function at the adopted magnitude limit. By using

both a brighter and fainter magnitude limit this is intended to capture the range over which a program’s detection probability function is transitioning.

It was found that use of different magnitude limits and a real detection probability for W84V (from recovery of embedded synthetic sources) made little difference to the resulting shape of the HDF in the application of the method. For this reason we don’t explore this further.

3.2. Results

For each observation the analysis consists of computing the volume correction factor V_{ijk} , as defined in section 2.5, given the apparent magnitude, magnitude limit, geocentric distance, and orbit parameters for each NEA observation-night and using a value of 0.02 AU for the pseudo-parameter d_{min} . In addition, for program W84V the known detection probability distribution (P in eqn. 2) was applied. (The detection probability makes only a small difference in the results showing that it is a minor effect compared to the orbit volume factor z in eqn. 2). Figure 6 shows the factors as a function of H -magnitude separated by program.

The first feature to notice is the scatter plots are fairly similar. Note the log scale such that, for example, a value of 4 means that it represents 10^4 other NEAs with the same orbit at various distances including beyond the detection limit near aphelion.

The extreme points seen in fig. 6 produce very large contributions for a small number of observations. These points are often large because of poor or uncertain magnitude measurements (which are particularly prevalent at the very bright and faint ends) and sometimes due to large eccentricities with aphelions unusually far away. Such extreme ampications by a small number of observations have an impact on the HFD results. To understand why consider computing an unbinned cumulative distribution by ordering the points in H and making a point-by-point cumulative sum. This generally produces a smooth shape except at the points with extreme corrections which add large discontinuous jumps. In between these jumps the log slope continues on with the same slope as before the jump.

To minimize this distorting effect of a very few points we introduce an upper limit to the correction factors as indicated by the lines in fig. 6. We can apply this line either by adjusting the values down to the limit or by eliminating them from the analysis. The results presented here use the former but are essentially identical if the NEA observations are excluded entirely. The limit lines are all identical so as to minimize biases and implicit parameters. In keeping with having only the single magnitude limit parameter, the identical lines are simply shifted by the magnitude limit parameter for each program.

While justified because these are often magnitude errors, modifying these small number of points may seem ad hoc. Therefore, the results are computed both with and without the limits (discussed later and shown in fig. 9c).

Each HFD derived from a sample has a similar shape but a different normalization. Without making adjustments the scatter between the samples would be

dominated by this. If one simply normalizes at a particular H -magnitude then the scatter would be zero at that point. Instead a power law slope is fit to each sample HFD over the range $H=[21:25]$, where the number of NEAs contributing is largest, and the fit is evaluated at $H=22$. All the samples being combined are then normalized to a log value of 5.3 and the mean and standard deviation is computed to form the HFD across the combined samples. Note we are not constraining the shape of the HFD in this process.

Figure 7 shows the HFDs combined by program. The error bars are 3 standard deviations which essentially describe the scatter in the samples. The reference solid line is the same in all HFD plots presented in this paper and is ultimately the final result we quote:

$$\log(N_{\text{nea}<H}) = 0.5H - 5.7 \quad (4)$$

It is a power law with a slope of one-half and a normalization that asymptotes to the nearly complete number of large NEAs (> 2 km). The results for each program look very similar and in agreement with the standard HFD of eqn. 4.

A power law slope is determined for each program using the means and error bars from the subsamples in the range $H=[18:27]$ (a larger range than for the normalization of the subsamples previously noted). The values for these slopes are reported in table 1.

The agreement between different programs can be seen in figure 8. This plots the mean values for the HFDs in program set 1 at each magnitude. The H -magnitude bin positions are shifted along the standard 0.5 power law of eqn. 4 so the values can be more clearly seen. For clarity only set 1 and no error bars are shown. This reinforces the conclusion that different programs agree well with a simple HFD for the NEAs and we can proceed to combine all the samples across all the programs.

Figure 9a combines all subsamples from program set 1 (the darker filled symbols) and for sets 1 and 2 together (the lighter open symbols). The points for the two combinations are offset along the standard line so the two don't overlap. The error bars are 2 standard deviations. The power law slopes fit to these combinations are reported at the bottom of table 1. The additional lines in the figures will be discussed later.

The only ad hoc element in this analysis is the upper limit, shown in fig. 6 and discussed earlier, placed on the volume corrections. These cause large distortions in the cumulative counts by a very small number of observations. To evaluate whether this affects the results, the analysis was also performed without this limit; i.e no rejection or alterations to the full dataset including extreme outliers. The effect of not applying a limit is an increase in the scatter of the subsamples as shown in fig. 9b. This does not constrain the slope of the distributions very well but it clearly shows a simple power law, consistent with eqn. 4, is most likely and is not consistent with their being structure in the HDF of the form seen in HSGT.

3.3. Undiscovery Simulation

A study with population models and simulated observation strategies would be valuable to see if the method recovers the input population but that is beyond the scope of this paper. However, there is a simple simulation that can address a particularly important question:

Is there is something in the methodology that forces a simple power law?

The simulation, which is more in the nature of an experiment, consists of randomly "undiscovering" a subset of NEAs. The reason for using an undiscovery simulation is that no orbits or detection strategies have to be created. We are just saying those orbits and magnitudes/sizes don't exist in the simulated full population and so are not discovered and added to the catalog of known NEAs. Any pattern of undiscoveries that is not uniform in absolute magnitude but blind to orbital parameters can be used to answer the question.

The pattern we use is a gaussian probability distribution that preferentially undiscovers NEAs around $H=22$. The undiscovery probability distribution used in this simulation is shown by the dotted line and right-hand axis in figure 10a. This distribution has a particular significance as will be discussed later. Randomly undiscovering these NEAs produces the simulated known NEA population given by the dashed line in figure 10b. The random undiscovery was over the full catalog of known NEAs with no selection by orbit, whether a NEA was observed by a particular program, or within the opposition window. The analysis performed on the complete known NEA population (the solid line in fig. 10b) is repeated with the simulated known population. The HFD result is shown in figure 9c.

As seen in the figure, the result is no longer a structureless power law. Rather it has a dip that is, by design, a good approximation to the HFDs of HSGT. Note, however, that the intent of this simulation is to answer a question about the methodology and not to try and explain the HSGT structure. There is no physical basis or claim in the undiscovery simulation related to why that structure is found by HSGT.

The answer to the question posed in this section is then:

*The methodology described in this paper does **not** force the simple power law found using the complete catalog of known NEAs!*

4. Discussion

This analysis, based solely on observations and the catalog of known NEA orbits derived from them, along with some basic assumptions, leads to the simple and robust result that the cumulative absolute magnitude frequency distribution of near-Earth A^3 asteroids (HFD) is a power law with the intriguing slope of 0.5. The only sign of a departure from this is for the faintest, smallest, and hardest to find NEAs where the number of known examples is limited.

It is tempting to just present this result as it stands. However, the difference with respect to HSGT immediately draws attention from anyone familiar with those studies. This difference is also important for estimating the challenges in the planetary defense mandate for finding most of the NEAs larger than 140m. So we address this "elephant in the room".

Figure 9 includes the HFDs from the commonly cited studies. Brown et al. (the dashed) line provides a consistency check with bolide observations. That work suggests a power law slope of 0.54 for the smallest NEAs (those which impact the Earth). This is not too dissimilar to the slope found in this study. The authors indicate that this slope connects to the slightly larger NEAs. In the figure the slope is connected around $H=25$.

Where a significant discrepancy is seen is in the studies of HSGT whose HFDs are also shown in the panels of fig. 9. At a coarse level the overall slopes and tendency to reach similar cumulative numbers for the smallest NEAs is in reasonable agreement. However, the notable feature is a dip in the range $H=[20:26]$.

To more clearly quantify the magnitude of the difference, figure 10a displays the ratio (in non-cumulative linear units) of the Harris and D'Abramo distribution to the simple $\alpha = 0.5$ power law of this study. This shows a difference of up to 700% at $H=22$ ($\sim 100m$). This ratio can vary by a small amount depending on the details of the normalization which is at $H=16$ in this case. As seen in fig. 9, the Schunová-Lilly et al., Granvik et al., and Tricarico ratios would be similar.

An argument typically used to justify the reality of this dip is that there is also a dip in the raw numbers of discovered NEAs in approximately the same range of magnitudes. Harris and D'Abramo claim this makes their result definitive. To consider this we can look at figure 10b that plots the histogram of the known NEAs. There is, indeed, an apparent dip in what might be expected in the range $H=[21.5:25]$ if we *assume* the histogram should look like a single peak or plateau, but it could equally well be a superposition to two peaks. Many people have speculated on possible reasons for this histogram as both indicative of something in the true population (e.g. a rubble pile to monolithic transition) or a discovery selection effect (e.g. a transition between fast versus slow discovery methods).

The deficit relative to a plateau or gaussian (shown as extrapolations with dotted lines) at $H=22.75$ is in the range [22%:37%]. While one could attempt to link this to the factor of 700% in fig. 10a this seems to be a somewhat extreme amplification. While the undiscovery simulation (§3.3) is not a physical explanation, the particular undiscovery probability distribution used (fig. 10a) can be considered in the context of this argument. In order for the method developed in this paper to find a dip of the size in the HSGT HFDs, assuming it is caused by a deficit in discovered asteroids, requires the much more significant deficit shown in fig. 10b.

So why doesn't the structure around $H=22$ in the histogram of known NEAs affect the HFD in this study? The obvious answer is that the method yields the true population distribution from the sample just as it accounts for a steadily

increasing number of NEAs at small H -magnitudes despite the fact that the discovery histogram is declining there.

One might be tempted to discount this study and give greater weight to the HFDs of the HSGT studies, as well as the derivative version of Stokes et al. [10], because the latter studies are similar and outnumber this work. This is not the place to review those other studies. However, there are notable commonalities in the methodologies, beyond ultimately tying back to the catalog of known NEAs which all studies must do, which makes them less distinct than might be apparent. They all involve generation of a synthetic population at some point; either by sampling from a subset of known orbits or making use of the same population models of Bottke et al. [2] and Greenstreet et al. [5]. They also generally involve modeling of detection efficiencies of the surveys used in their analysis through various means including simulated surveys over the population models.

The method and result presented here likely raises several additional questions for the readers. These commonly asked questions are considered next. The answers lie in the three primary assumptions made earlier.

What about the different methods and sensitivities of the various programs and differences between survey vs. recovery focuses? As long as the entire community has discovered a fair sample of the true population the only thing that enters in the analysis is the observed magnitudes at specific times and orbital distances and an estimate of the magnitude limit for each measurement. Hence any observation could be used. Large programs, both survey and recovery oriented, are used simply because it is possible to estimate a magnitude limit from statistics of the reported measurements. A second aspect to this question is that this study is about the shape of the distribution; i.e. the relative numbers at different sizes. Most of the questions about survey methodology, area covered, cadences, etc. enter into the normalization which ultimately must tie to the bright end of the distribution.

What about albedos? As with the previous answer, unless albedo has affected the representative sample of NEAs in the catalog in some systematic way, albedo does not enter into the analysis at all. Whatever the albedo, and hence apparent magnitude at some distance, the method just makes use of the inverse square law to find the volume observable up to the program's limiting magnitude.

What about magnitude variability and rotation? It is true the magnitudes in the catalog contain variability, not only from physical effects but from measurement errors of various kinds. However, since each NEA is typically observed several times by different programs at different times, the principle of large number statistics average out the light curves.

5. Conclusion

This paper presents a method for estimating the population of near-Earth A^3 asteroids and their absolute magnitude distribution. It is solely based on

observations and simple assumptions rather than orbital population modeling. There are two clear conclusions.

The first is that the cumulative absolute magnitude distribution is a power law with a slope of 0.50 ± 0.03 . The simple form and value of the slope is strongly favored by an Occam's razor argument. There is nothing in the methodology that forces this result. It is also extremely robust.

The analysis was also performed with just the Apollo and Aten Earth crossing asteroids. The result was an identical power law distribution. This shows there is no significant difference caused by Earth crossings.

The second conclusion is that this method does not show the "dip" in the HFD found by other studies (e.g. HSGT). The importance of the difference between this study and those showing the dip is that the size range where the discrepancy is greatest (around 100m) is what the planetary defense initiative is hoping to catalog. A factor of ~ 7 would have a major effect on the scale of effort and time needed to achieve the discovery mandate.

6. Acknowledgements

This work is a synthesis of the many years of effort by many teams surveying the near-Earth asteroid population and the many observatories supporting them. It also depends on the compilation work of the Minor Planet Center.

References

- [1] L. Allen, D. Trilling, F. Valdes, C. Fuentes, D. James, D. Herrera, J. Rajagopal, B. Burt, and T. Axelrod. The DECam NEO Survey: A sensitive, wide-field search for near-Earth asteroids. In *AAS/Division for Planetary Sciences Meeting Abstracts #46*, volume 46 of *AAS/Division for Planetary Sciences Meeting Abstracts*, page 414.01, Nov. 2014.
- [2] W. F. Bottke, A. Morbidelli, R. Jedicke, J.-M. Petit, H. F. Levison, P. Michel, and T. S. Metcalfe. Debaised Orbital and Absolute Magnitude Distribution of the Near-Earth Objects. *Icarus*, 156:399–433, Apr. 2002. doi: 10.1006/icar.2001.6788.
- [3] P. Brown, R. E. Spalding, D. O. ReVelle, E. Tagliaferri, and S. P. Worden. The flux of small near-Earth objects colliding with the Earth. *Nature*, 420: 294–296, Nov. 2002. doi: 10.1038/nature01238.
- [4] M. Granvik, A. Morbidelli, R. Jedicke, B. Bolin, W. F. Bottke, E. Beshore, D. Vokrouhlický, D. Nesvorný, and P. Michel. Debaised orbit and absolute-magnitude distributions for near-Earth objects. *Icarus*, 312:181–207, Sept. 2018. doi: 10.1016/j.icarus.2018.04.018.
- [5] S. Greenstreet, H. Ngo, and B. Gladman. The orbital distribution of Near-Earth Objects inside Earth’s orbit. *Icarus*, 217:355–366, Jan. 2012. doi: 10.1016/j.icarus.2011.11.010.
- [6] A. W. Harris and G. D’Abramo. The population of near-Earth asteroids. *Icarus*, 257:302–312, Sept. 2015. doi: 10.1016/j.icarus.2015.05.004.
- [7] K. G. Malmquist. A contribution to the problem of determining the distribution in space of the stars. *Meddelanden fran Lunds Astronomiska Observatorium Serie I*, 106:1–12, Feb. 1925.
- [8] B. G. Marsden. The Minor Planet Center. *Celestial Mechanics*, 22:63–71, July 1980. doi: 10.1007/BF01228757.
- [9] E. Schunová-Lilly, R. Jedicke, P. Vereš, L. Denneau, and R. J. Wainscoat. The size-frequency distribution of $H > 13$ NEOs and ARM target candidates detected by Pan-STARRS1. *Icarus*, 284:114–125, Mar. 2017. doi: 10.1016/j.icarus.2016.11.010.
- [10] G. Stokes, B. Barbee, W. F. Bottke, M. W. Buie, S. R. Chesley, P. W. Chodas, J. B. Evans, R. E. Gold, T. Grav, A. W. Harris, R. Jedicke, A. K. Mainzer, D. L. Mathias, T. B. Spahr, and D. K. Yeomans. Update to Determine the Feasibility of Enhancing the Search and Characterization of NEOs. Technical report, Prepared by the Near-Earth Object Science Definition Team at the Request of the National Astronautics and Space Administration, 2017.
- [11] P. Tricarico. The near-Earth asteroid population from two decades of observations. *Icarus*, 284:416–423, Mar. 2017. doi: 10.1016/j.icarus.2016.12.008.

Table 1: Table of datasets.

ID	N_{neo}	N_{night}	Set	M_{lim}	α [18:27]
G96V - Mt. Lemmon Survey	6890	12440	1	22.5	0.54 ± 0.016
H21V - ARO , Westfield	6252	14895	1	23.0	0.45 ± 0.012
F51w - Pan-STARRS	5379	8990	1	23.0	0.50 ± 0.015
703V - Catalina Sky Survey	4248	9256	1	21.0	0.51 ± 0.011
926R - Tenagra II Obs.	3442	5813	1	22.0	0.47 ± 0.012
291R - LPL/Spacewatch II	3295	5618	2	23.0	0.53 ± 0.017
807R - CTIO	3091	6759	2	23.0	0.55 ± 0.022
J95R - Great Shefford	2906				
691V - SO KPNO/Spacewatch	2699	5827	2	22.5	0.52 ± 0.018
204R - Schiaparelli Obs.	2620				
474R - Mount John Obs.	2020				
568R - Mauna Kea	1832				
291V - LPL/Spacewatch II	1784	3728	2	23.0	0.56 ± 0.022
...	...				
W84V - DECam NEO Survey	512	1225	1	24.0	0.51 ± 0.013
...	...				
Set 1					0.50 ± 0.026
Set 1 + 2					0.51 ± 0.029

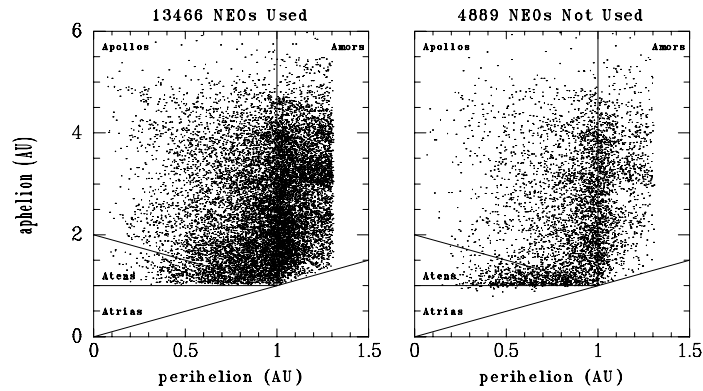


Figure 1: Scatter plot of aphelion vs perihelion distances of the known NEAs. The left and right plots separate the NEAs used and not used in the study. The criterion for being used are the program sets with large numbers of observation obtained within 30 degrees of opposition. The standard sub-classes of NEAs are indicated. These illustrate the known distribution of NEA orbits, that the fraction used in this study is large, and that those not used are not qualitatively different than those used.

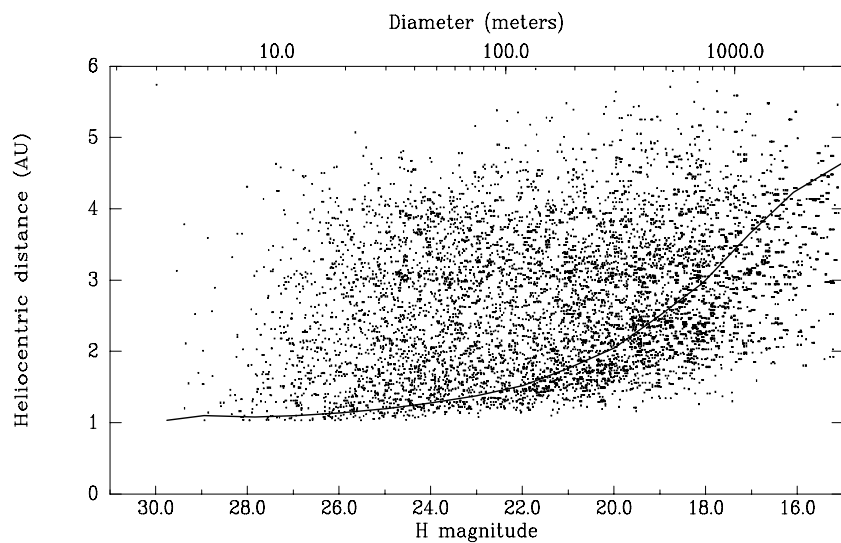


Figure 2: Scatter plot of aphelion distances for NEAs observed by the F51w program (Pan-STARRS w-band). In this plot a NEA, represented by each point, will traverse a vertical line down to its perihelion distance during its orbit. The solid line is the upper limit boundary of distance at which NEAs were observed by F51W. NEAs were only observed at distances below the line demonstrating that many NEAs will only be observable for a small part of their orbit in addition to the chance that they appear in the field of view of the program. Other programs are qualitatively similar with detection boundaries varying slightly by magnitude limit.

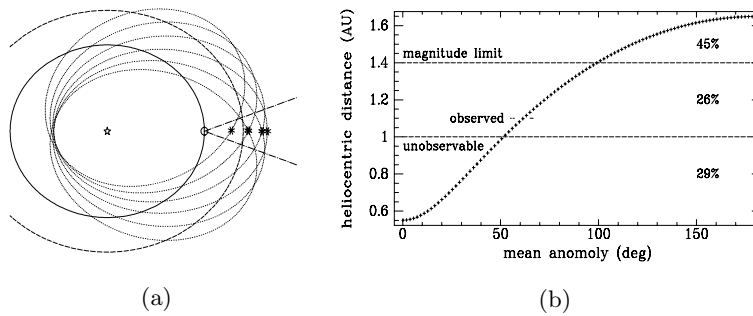


Figure 3: These diagrams illustrate the key concepts of the method. The example shows a representative NEA with $H=21.8$, $a=1.1\text{AU}$, and $e=0.5$ observed at a geocentric distance of 0.1AU and apparent magnitude of 22 by a program with a limiting magnitude of 22.5. (a) An ensemble of similar NEAs with the same orbital parameters and absolute magnitude observed within an opposition cone. The dashed line is the magnitude limit. (b) The heliocentric distances for the ensemble. The points are evenly sampled in mean anomaly which, by definition, is equivalent to evenly sampled in time. The density of points demonstrates that the NEAs are more likely to be near aphelion and the percentages are the fraction of time spent in the three regions (interior to the Earth, observable to the magnitude limit, and unobservable beyond the limiting magnitude). The figures are interpreted further in the text.

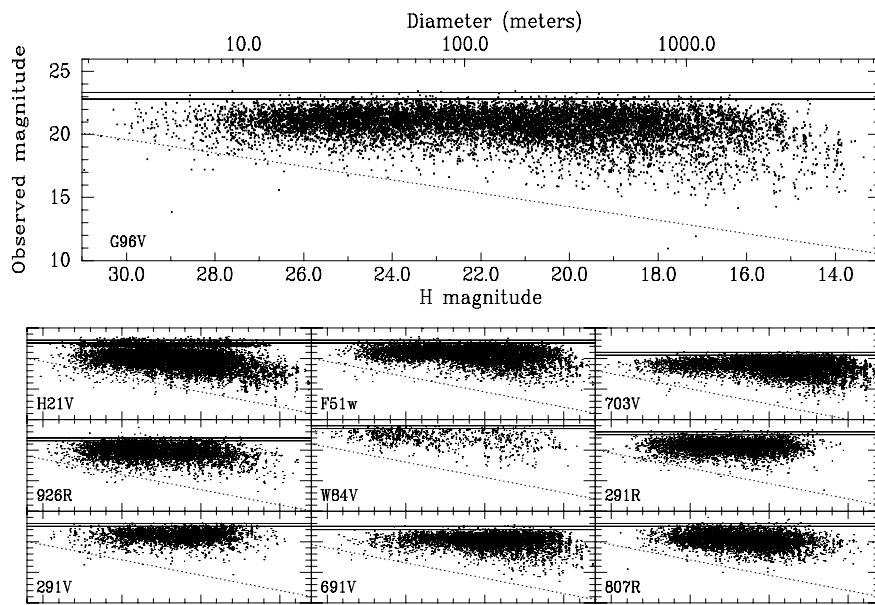


Figure 4: Distribution of observed magnitudes as a function of NEA absolute magnitude for programs included in this study. The solid lines at the upper boundary of apparent magnitude are the two magnitude limits (separated by 0.5 mag) adopted for each program. The dotted lines are just indicative of an expected trend that smaller NEAs are observed closer with a corresponding smaller volume such that they are rarely observed with bright apparent magnitudes. The lines have the same slope and are a fixed distance from the magnitude limit.

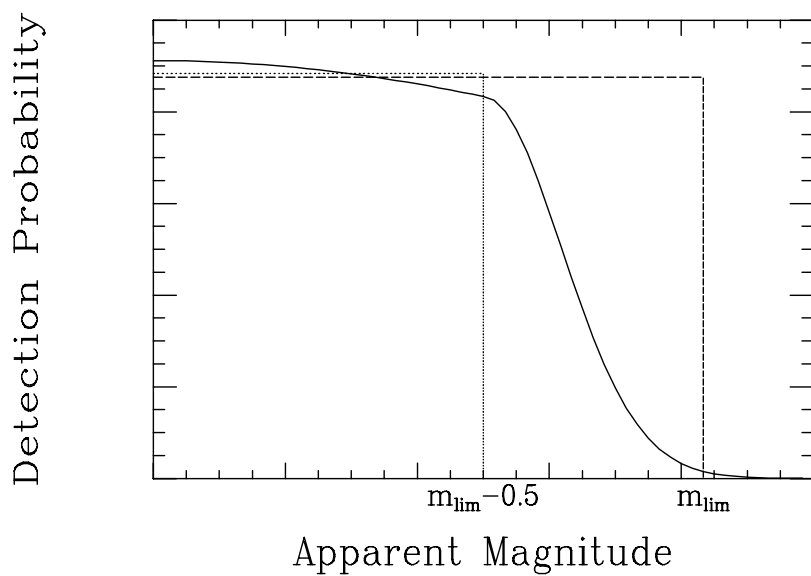


Figure 5: Illustration of the relationship between the two magnitude limits and the simplification of the detection probability P being constant up to the magnitude limit. If the true probability distribution is bracketed by the limits then it would be expected that the result using the true distribution would also be bracketed. Note that an actual probability distribution was used for the W84V program in this study.

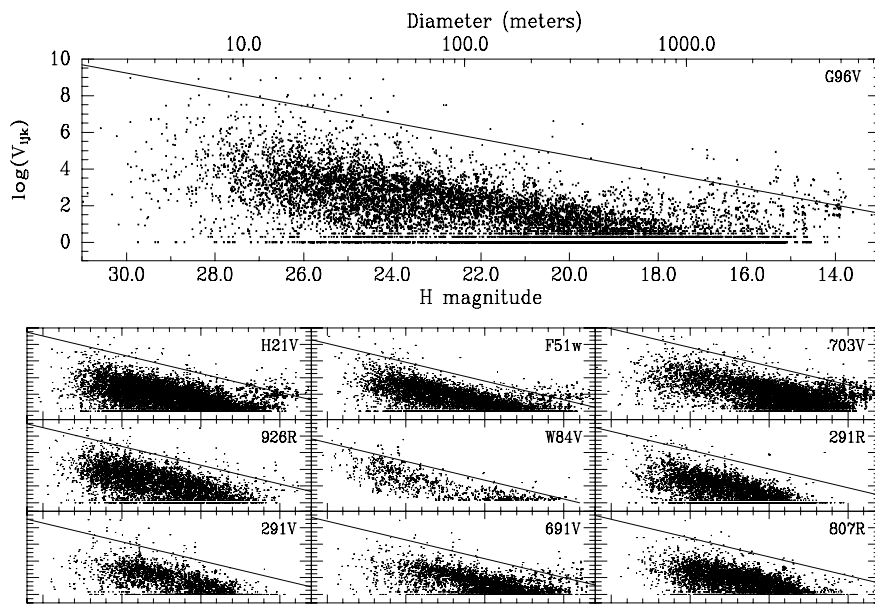


Figure 6: Distribution of the volume corrections as a function of NEA absolute magnitude for programs included in this study. The solid line is a limit applied to avoid gross effects from a small number of observations with either poor absolute magnitudes or extreme ellipticities. The limits all have the same slope and the origin is tied to the magnitude limit parameter so that each program is treated the same. Note that the curves look qualitatively similar with no obvious differences in the range $H=[20:25]$.

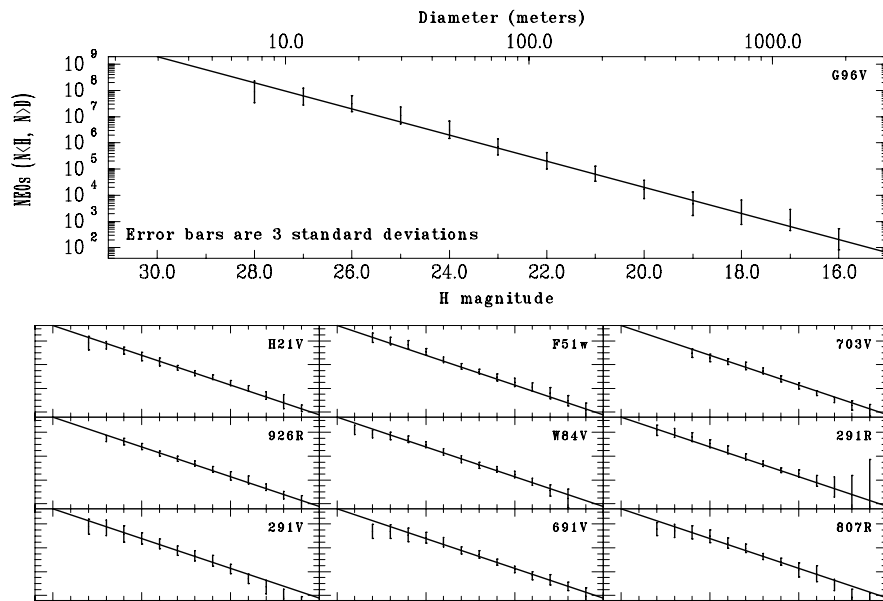


Figure 7: The HFD means with three standard deviation error bars for each program. The solid lines are the standard $\alpha = 0.5$ power law conclusion of this study.

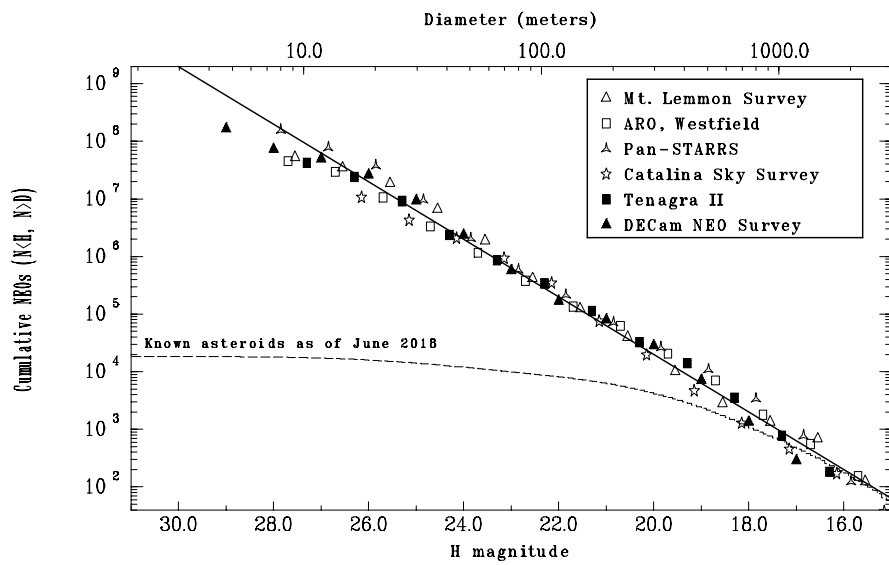


Figure 8: The mean values for each program in set 1 are plotted with the solid line showing the standard $\alpha = 0.5$ HFD conclusion of this study. The dashed line is the cumulative distribution of the known NEAs. For clarity the positions of the points are shifted along the 0.5 power law, program set 2 is not included, and the error bars are omitted.

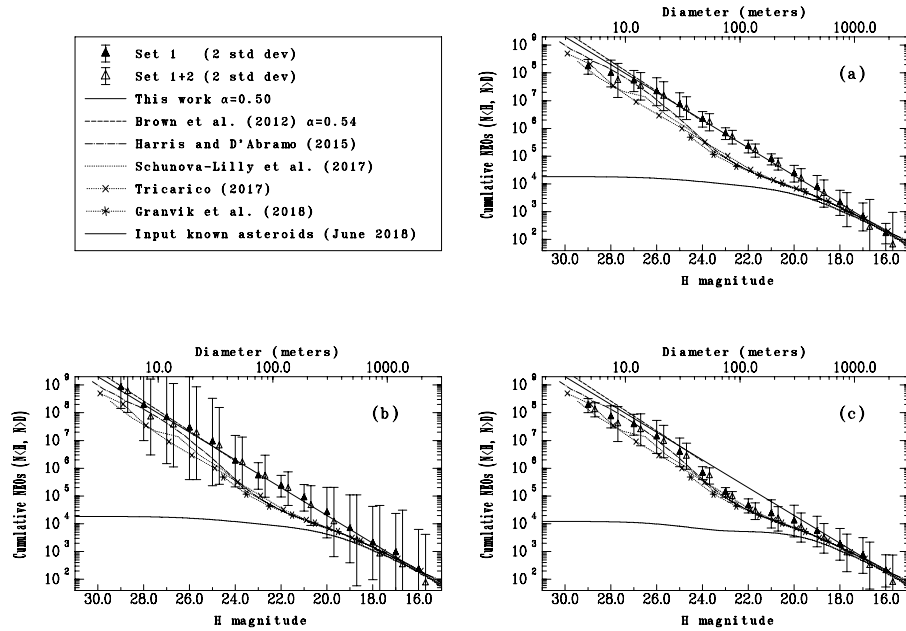


Figure 9: NEA HFDs from this and other studies. The HFDs are normalized to asymptote to the largest known NEAs. The heavy solid line is the $\alpha = 0.5$ conclusion of this study. The other HFDs are as indicated in the legend. (a) Mean and two standard deviation error bars based on multiple subsamples across multiple programs. The darker, filled error bars are from the set 1 programs and the lighter open error bars, offset along the $\alpha = 0.5$ line for clarity, are from all programs included in this study. The contribution from a small number of outlier NEAs have been limited as discussed in the text and shown in fig. 6.. (b) The error bars are computed in the same way as in (a) except there is no adjustment for outlier NEAs. (c) The error bars are computed in the same way as (a) except the input catalog of known NEAs is modified by "undiscovering" some of them as described in §3.3. This is a simulation illustrating the $\alpha = 0.5$ result is not a forgone consequence of the method.

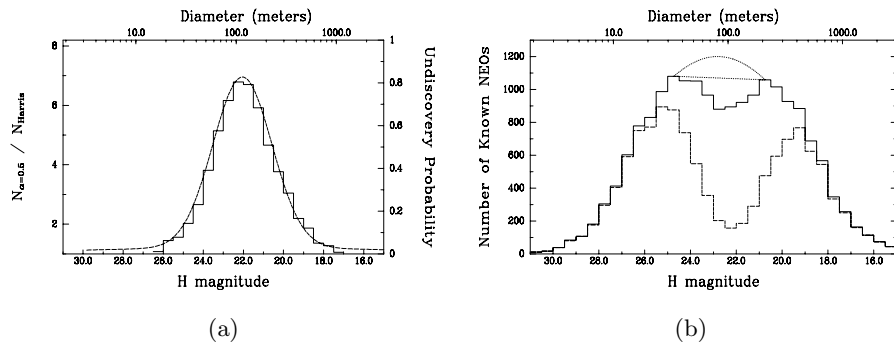


Figure 10: (a) The solid binned line and left axis is the ratio of the $\alpha = 0.5$ (this work) to the Harris and D'Abramo (non-cumulative) histograms normalized to be equal at $H=16$. The dashed line and right axis is a probability distribution for discovered NEAs to be "undiscovered" in a simulation. (b) The solid line is the histogram of discovered NEAs as of June 2018. If one assumes the shape should not be bimodal then the dotted lines extrapolate a plateau and gaussian for characterizing a possible discovery deficit. The dashed line is a histogram with known NEAs "undiscovered" using the probability distribution in (a) for the simulation described in §3.3.